International Journal of Engineering Research and Science & Technology

ISSN : 2319-5991
Vol. 1, No. 2
April 2015

2nd National Conference on "Recent Advances in Science Engineering & Technologies" RASET 2015

Organized by

Department of EEE, Jay Shriram College of Technology, Tirupur, Tamil Nadu, India.

www.ijerst.com

Email: editorijerst@gmail.com or editor@ijerst.com

International Journal of Engineering Research and Science & Technology

ISSN 2319-5991 www.ijerst.com
Special Issue, Vol. 1, No. 2, April 2015
2nd National Conference on "Recent Advances in Science, Engineering&Technologies" RASET-2015

Research Paper

FUZZY BASED SOLAR PHOTOVOLTAIC WATER PUMPING SYSTEM USING INDUCTION MOTOR

R Praveena[1]* and N Ramayarani[1]

*Corresponding Author: ***R Praveena*** ✉ praveenaraj5@gmail.com

This paper presents water pumping system using renewable source solar photovoltaic without the use of chemical storage batteries. In this work, Two Inductor boost converter (TIBC) is designed to drive the three phase induction motor through three phase voltage source inverter (VSI). TIBC converter is also known as current fed multiresonant converter having high voltage gain and low input current ripple. Converter switches are controlled through hysteresis controller and ZCS resonant topologies that are used for active switches and diode rectifiers. Solar PV power fluctuates according to irradiation level of sunlight and hence tracking of maximum power at all time is mandatory. So the Perturb and observe (P&O) method is applied here to track maximum power. In this paper Fuzzy controller is used to minimize the error and hence the efficiency of whole system improved. The proposed method is verified with MATLAB/SIMULINK and comparisons between PI & Fuzzy are also analyzed in this paper.

Keywords: TIBC-Two inductor boost converter, VSI- voltage source inverter,P&O -Perturb and Observe, MPPT- Maximum power point tracking

INTRODUCTION

Lack of electricity is one of the main troubles in the development of rural India. India's grid system is considerably under developed, with major sections of its populace still surviving off-grid. Hence standalone system is most welcome and necessary in rural area of India. Moreover, environmental issues such as population and global warming effects are driving researchers towards the development of renewable energy sources including solar systems.

One of the most beneficial applications of PV standalone systems is water pumping, particularly in rural areas that have a considerable amount of solar radiation and have no access to national grids. Indeed an effective solution must ensure that the PV generator runs at the maximum power point (MPP) and that the motor runs at a high efficiency level. Solar power systems need MPPT because it reduces the solar array cost by decreasing the number of solar panels needed to obtain the desired output power.

The batteries allow the motor and pump system to always operate at its rated power even in temporary conditions of low solar radiation. This facilitates the coupling of the electric dynamics

[1] Department of Electrical and Electronics Engineering, Sri Krishna College Of Engineering and Technology, Coimbatore.

of the solar panel and the motor used for pumping [8]. Generally, the batteries used in this type of system have a low life span, only two years on average [8], which is extremely low compared to the useful life of 20 years of a PV module. The cost of installation and maintenance of such, systems are substantially high. Also, the lack of battery replacement is responsible for the failure of such systems in isolated areas. The majority of commercial systems use low-voltage dc motors, thus avoiding a boost stage between the PV module and the motor [9]. Lower efficiency and higher maintenance cost of DC motor compared to induction motors and are not suitable for applications in isolated areas. Another problem is that low-voltage dc motors are not ordinary items in the local markets. Because of the aforementioned problems, this work based on use of a three phase induction motor, due to its greater robustness, lower cost, higher efficiency, availability in local markets, and lower maintenance cost compared to other types of motors. The design of a motor drive system powered directly from a PV source demands optimum solutions to face the challenge of operating under variable power restrictions and still maximize the energy produced by the module and the amount of water pumped [10]. And this requirements demand the use of a converter with the following features: high efficiency—due to the low energy available, low cost—to enable its deployment where it is most needed, autonomous operation—no specific training needed to operate the system, robustness—minimum amount of maintenance possible; and high life span—comparable to the usable life of 20 years of a PV panel.

This paper proposes a new dc/dc converter and control suitable for PV water pumping and treatment that fulfill the requirements of the aforementioned features.

This paper is organized as follows section II about the existing method; section III describes the proposed method, section IV giving detailed explanation operational conditions of converter. Section V describes the designing of photovoltaic panel; section VI about the controllers for the whole system, section VII discuss about the expected result.

EXISTING METHOD

The existing method of the solar water pumping system worked with DC motors. And [1] they used induction motor for pumping water. In that paper they have used PI controller with Hill Climbing MPPT tracking technology. They achieved better performance in converter voltage gain and analyzed the performance of system. In this, paper analyzing the system using Fuzzy with Perturb & Observe for minimizing the error and for improving the precise control of duty cycle.

PROPOSED METHOD

To meet the requirement of the proposed system, it was designed to use a single PV module Fig.3.1 presents an overview of the proposed system. The energy produced by the panel DC is fed to the induction motor through a converter with two power stages: a dc/dc two-inductor boost converter (TIBC) stage to boost the voltage of the panels and a dc/ac three-phase inverter to convert the dc voltage to three-phase ac voltage. The inverter is based on a classic topology (three legs, with two switches per leg) and uses a sinusoidal pulse width modulation (PWM) (SPWM) strategy with 1/6 optimal third harmonic voltage injection as proposed in [9]. The use of this PWM strategy is to improve the output voltage

level as compared to sinusoidal PWM modulation. This is a usual topology, and further analyses on this topology are not necessary. For the prototype used to verify the proposed system, a careful selection of the voltage source inverter (VSI) components is more than enough to guarantee the efficiency and cost requirements.

Figure 1: Block Diagram of Whole System

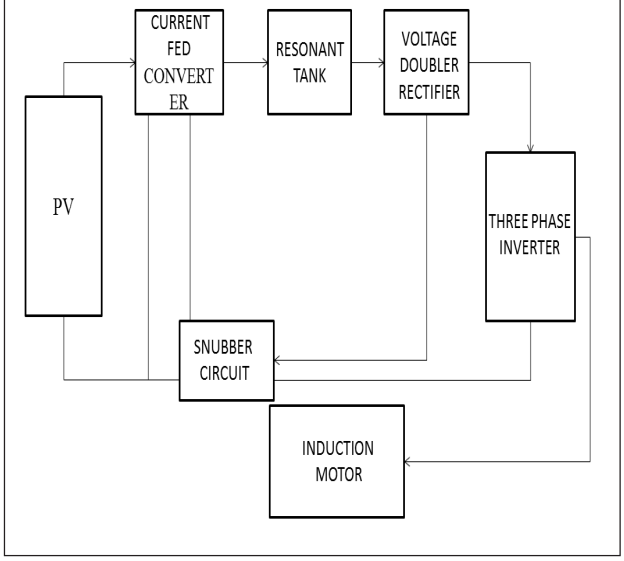

This kind of system needs DC/DC converter with high voltage gain it large voltage conversion ratio because of low output voltage from PV panels and small input ripple current so that it does not produce any oscillation over the maximum power point. The commonly used isolated voltage-fed converters normally have a high input current ripple, which forces the converter to have large input filter capacitors. These are normally electrolytic, which are known to have a very small lifetime and thus affect the overall life span and mean time before failure of the converter. Furthermore, the inherent step-down characteristic of the voltage-fed converters, the large transformer turns ratio needed to boost the output voltage, the high output diode voltage stress, and the need of an *LC* output filter make voltage-fed converters not the best choice for this application.

When compared to the voltage-fed topologies, current-fed converters have some advantages. Current –fed converters usually have an inductor at the input, so the system can be sized to have input current ripple as low as needed, thus eliminating the need of the input capacitor at the panel voltage. It normally derived from the boost converter, having an inherent high step-up voltage ratio, which helps to reduce the needed transformer turns ratio. The classical topologies of this kind are the current-fed push–pull converter [14], [15], the current-fed full-bridge [16], and the dual half-bridge converter [17]. Although the current-fed topologies have all the above mentioned advantages, they still have problems with high voltage spikes created due to the leakage inductance of the transformers and with high voltage stress on the rectifying diodes. One of the solutions to the current-fed PWM converters is the use of resonant topologies able to utilize the component parasitic characteristics, such as the leakage inductance and winding capacitance of transformers, in a productive way to achieve zero current switching (ZCS) or zero voltage switching (ZVS) condition to the active switches and rectifying diodes.

In this paper, the use of a modified TIBC for the first-stage dc/dc converter is proposed. Due to its very small number of components, simplicity, high efficiency, easy transformer flux balance [20], [21], and common ground gate driving for both switches, these features make it the perfect choice for achieving the system's necessary characteristics. Apart from the high dc voltage gain of the TIBC, it also compares favorably with other current-fed converters concerning conduction losses, switch voltage

stress, and transformer utilization [20], [21]. In extension, the input current is distributed through the two boost inductors having its current ripple amplitude halved at twice the PWM frequency. This last feature makes the oscillations minimization at the PV module operation point and makes it easier to achieve the MPP.

In its classical implementation, the TIBC is a hard-switched overlapped pulse-modulated converter; this way, at least one of the switches is always closed, creating a conduction path for the input inductor current. Not the less, the TIBC can be modified to a multiresonant converter by adding a capacitor at the transformer's secondary winding [22], [23]. A multiresonant tank is built by the magnetizing inductance of the transformer, its leakage inductance, and the added capacitor, as shown in Fig.4.2. The intrinsic winding capacitance of the transformer is included in the resonant capacitor. To achieve ZCS condition for the input switches and output rectifying diodes by adding this capacitor and using the parasitic components of the transformer. And this enables the converter to operate at high frequencies with greater efficiency.

With the use of a voltage doubler rectifier at the secondary side of the transformer, as shown in Fig.4.2, it is possible to reduce the transformer turns ratio, the necessary ferrite core, and the voltage stress on the MOSFETs to half of the original ones. As a result, the transformer is cheaper, the MOSFETs are cheaper, and the number of diodes in the secondary side is halved. Also, the output dc bus capacitor can be integrated with the capacitors of the rectifier, particularly because the second stage three-phase VSI has almost dc input current, exempting the bus capacitor from any ac decoupling current. Classically, the TIBC have a minimum operation load to maintain an established output voltage. Below a certain load level, the energy transferred to the output capacitor is not completely transferred to the load and causes an increase in the output voltage. This happens because the inductors are charged even if there is no output current. As a result, this converter has a drawback when used in motor drive systems. Since the motor is a variable load and it has large time constants, it will demand low power at some operation points, i.e., at low speed and startup/ stop transients. As a result, a nondissipative regenerative snubber circuit is presented.

Two diodes and a capacitor connecting the input side directly to the output side of the converter makes the regenerative snubber circuit, as shown in Fig. 4.2. This makes it a nonisolated converter, which has no undesirable effect in the PV motor driver applications. The voltage over the MOSFETs is providing to a capacitor connected to the circuit ground, and the voltage of this capacitor is coupled in series with the output of the rectifier. Thus makes energy to be transferred from the input directly to the output, through the snubber, without going through the transformer, so that it reducing size and improving even more the efficiency of the converter. A modification in the control strategy of the proposed converter is also proposed. The perfect design of converter voltage gain makes its able to operate with constant gain for the application of a PV water pumping system, using a fixed duty cycle modulation for the primary switches. Hysteresis controller is use to solve the minimum load condition for the dc output voltage of the first stage is proposed. Both primary

switches are turned off when operating below the minimum required load, an uncontrolled increase of output voltage will be seen, and once this voltage reaches the upper threshold. With the added snubber, even with both switches turned off, there is still a path for the input inductors' current. And that energy is directly transferred to the snubber capacitor *Cs*. Minimum voltage increase during this hysteresis action so that capacitor must to size according that condition. As this capacitor is in series with the output rectifier, the same voltage increase will be esteemed in the output voltage. After the switches are turned off and the input inductors' energy is transferred to the snubber, thus the output voltage will start to decrease. Finally it reaching the lower hysteresis threshold and restarting the PWM operation with the fixed duty cycle.

OPERATION PRINCIPLE

To simplify the analysis of the proposed converter, the following assumptions need to be true during a switching interval: The input inductors *Li*1 and *Li*2 are sufficiently large so that their current is almost constant; the capacitors *Co*1, *Co*2, and *Cs* are large enough to maintain a constant voltage; and the output capacitors *Co*1 and *Co*2 are much larger than *Cr* to clamp the resonant voltage. In the hard-switched operation of the TIBC, the two primary switches *Q*1 and *Q*2 operate at an overlapped duty cycle switching scheme to guarantee a conduction path for the primary inductor current. When both *Q*1 and *Q*2 are turned on, *Li*1 and *Li*2 are charged by the input energy. When *Q*1 (*Q*2) is opened, the energy stored in *Li*1 (*Li*2) is transferred to *Co*1 (*Co*2) through the transformer and the rectifier diode *Do*1 (*Do*2).

Figure 2: Circuit Diagram of Proposed Converter

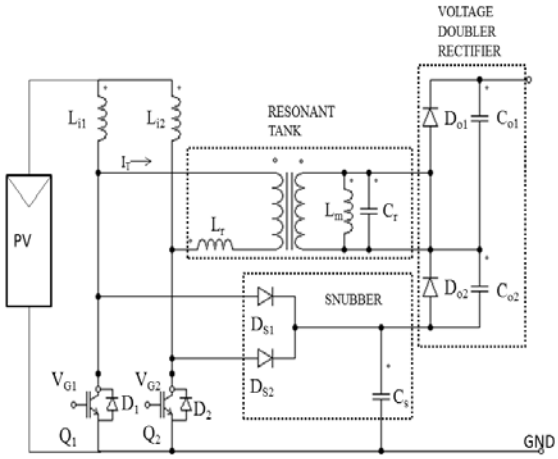

Once the multiresonant tank is introduced, two different resonant processes occur: 1)When both switches are closed, the leakage inductance *Lr* participates along with capacitance *Cr* in the resonance at the primary current switching and current polarity inversion, allowing ZCS operation for the primary switches, and 2) during the conduction time interval (between *t*4 and *t*5 in Fig. 3), when at least one of the switches is open, *Lr* is associated in series with *Li*1 or *Li*2, not participating on the transformer's secondary current resonance, formed only by *Lm* and *Cr*. The key waveforms for a switching period of the TIBC are presented in Fig. 3. In this figure, *VgQ*1 and *VgQ*2 are the gate signals of the switches *Q*1 and *Q*2, respectively; *VdsQ*2 is the drain-to-source voltage of MOSFET *Q*1; *IQ*2 is the current of MOSFET *Q*2; *VT* is the voltage at the primary of the transformer; *IT* is the current at the primary of the transformer; *ILi*1 and *ILi*2 are the currents of inductors *Li*1 and *Li*2, respectively; and *I*in is the input current of the converter and also the current supplied by the PV panel.

Mode 1: At time *t*1, the rectifying diode *Do*1 is already conducting, and the voltage on resonant capacitor *Cr* is clamped at +*V*out/2. At this instant, the switch *Q*1 is activated by *VgQ*1. As the switch is turned on, its voltage drops to zero, and the snubber diode *Ds*1 is forced to stop conducting. From *t*1 to *t*2, *Cr* transfers its energy to the leakage inductance *Lr*, beginning the primary switch's resonant process and forcing the current *IQ*2 on the switch *Q*2 to decrease.

Mode 2: At the time *t*2, the rectifying diode*Do*1 stops conducting, and *Cr* continues to resonate with the magnetizing inductance *Lm*. From *t*2 to *t*3, the primary switch's resonance (*Q*2) continues to force its current to decrease until it reverses its polarity. When *IQ*2 is negative, the switch can be turned off. This happens at instant *t*3 when *VgQ*2 is forced to zero.

Mode 3: At the time *t*3, the voltage *VdsQ*2 starts to increase, *Q*2 is completely blocked, and the snubber diode *Ds*2 begins to conduct, transferring energy directly to the snubber capacitor *Cs*. Between *t*3 and *t*4, *Cr* and *Lm* continue to resonate, decreasing the voltage on the doubler rectifier's input and on *VCr*. At instant *t*4, the voltage across *Cr* reaches "*V*out/2, and the rectifying diode *Do*2 starts to conduct, clamping *VCr* in"*V*out/2.

Mode 4: From *t*4 to *t*5, the capacitor *Co*1 is charged, and the current of *Do*2 starts to decrease.

Mode 5: At the instant *t*5, *Q*2 is turned on, initiating the resonant process on *Q*1. As *Q*2 is activated, *Ds*2 is forced to stop conduction.

Mode 6: At the instant *t*6, the current in *Do*2 reaches zero, and *Do*2 stops conducting, reinitiating the resonance between *Cr* and *Lm*. From this moment, until the end of the switching period, the process repeats symmetrically as explained for the other input switch.

The resonant process affects the output voltage, depending on the resonant tank component values and the load; this can be neglected because of its small influence and complex effect. Thus, neglecting the resonant effect over the output voltage, including the voltage doubler rectifier and the snubber connecting the primary and the secondary side of the converter, the static voltage gain (*Kv*) of the converter is defined as

$$\frac{V_{out}}{V_{in}} = K_v = \frac{1}{1-D}\left(\frac{N_s}{N_P}+1\right) \qquad ...(1)$$

where *D* represents the duty cycle of each switch and must be higher than 50% to guarantee the necessary overlapping for the correct operation. *Ns/Np* represents the transformer turns ratio.

PV DESIGN CHARACTERISTICS

Figure 3.1 shows the equivalent circuit of the ideal photovoltaic cell. The theory of semiconductors that mathematically describes the basic equation for I-V characteristic of the ideal photovoltaic cell is

$$I = I_{pv,\,cell} - I_{O,\,cell}\left[\exp\left(\frac{qV}{akT}\right)-1\right] \qquad ...(2)$$

The basic equation (5.1) of the elementary photovoltaic cell does not represent the I-V characteristic of a practical photovoltaic array. Practical arrays are composed of several connected series photovoltaic cells and the observation of the characteristics at the terminals of the photovoltaic array requires the inclusion of additional parameters to the basic equation.

Figure 5.1: Equivalent circuit of a practical photovoltaic device including the series and parallel resistances

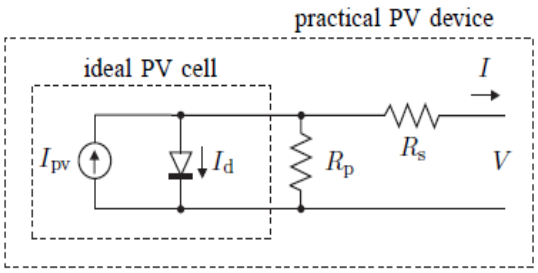

$$I = I_{pv} - I_O\left[\exp\left(\frac{V + R_s I}{V_t a} - 1\right)\right] - \frac{V + R_s I}{R_p} \quad ...(5.2)$$

Where, $V_t = N_s kT/q$

Cells connected in series provide the greater output voltage and cells connected in parallel increase the current. If the array is composed of N_p parallel connections of cells the photovoltaic and saturation currents may be expressed as: $I_{pv}=I_{pv}$, cellNp, $I_0=I_0$, cellNp. In (5.2) Rp is the equivalent parallel resistance and R_s is the equivalent series resistance of the array. Three remarkable points are highlighted: short circuit (0, I_{sc}), maximum power point (V_{mp}, I_{mp}) and open-circuit (V_{oc}, 0).

The practical photovoltaic device presents a hybrid behavior, which may be of current or voltage source depending on the operating point. The practical photovoltaic device has a parallel resistance R_p with stronger influence in the current source region of operation and series resistance R_s whose influence is stronger when the device operates in the voltage source region. The R_s resistance is the sum of several structural resistances of the device. The R_p resistance exists due to the leakage current of the p-n junction and also depends on the fabrication method of the photovoltaic cell. The value of R_p is generally high and some authors neglect this resistance to simplify the model. The value of R_s is very low and sometimes this parameter is neglected too [25], [26].

I-V characteristic of the photovoltaic device mainly depends on the internal characteristics of the device (R_s, R_p) and on external influences such as irradiation level and temperature. Generation of charge carriers and consequently the current generated by the PV depends on the amount of incident light directly falls on it. The light-generated current (I_{pv}) of the elementary cells, without the influence of the series and parallel resistances, is difficult to determine. Datasheets only inform the nominal short-circuit current ($I_{sc,n}$), which is the maximum current available at the terminals of the practical device. The assumption I_{sc} H" I_{pv} is generally used in photovoltaic models because in practical devices the parallel resistance high and the series resistance low. The light generated current of the photovoltaic cell depends linearly on the solar irradiation and is also influenced by the temperature according to the following equation

$$I_{pv} = \left(I_{pv} + K_i \Delta T\right)\frac{G}{G_n} \quad ...(5.3)$$

where, $I_{pv,n}$ [A] is the light-generated current at the nominal condition (usually 25^{0}C and 1000W/ m2), $\Delta T = T - T_n$.

The diode saturation current I_o and its dependence on the temperature may be expressed by

$$I_{O,n} = I_{O,n}\left(\frac{T_n}{T}\right)\exp\left[\frac{qEg}{ak}\left(\frac{1}{T_n}-\frac{1}{T}\right)\right] \quad ...(5.4)$$

where Eg is the band gap energy of the semiconductor (Eg H ≃ 1.12 eV for the polycrystalline Si at 25^0C [11] and $I_{o,n}$ is the nominal saturation current

$$I_{O,n} = \frac{I_{sc}}{\exp\left(\frac{V_{OC,n}}{aV_{t,n}}-1\right)} \quad ...(5.5)$$

The saturation current I_0 of the photovoltaic cells that compose the device depend on the saturation current density of the semiconductor (J_0, generally given in [A/cm^2]) and on the effective area of the cells. The current density J_0 depends on the intrinsic characteristics of the photovoltaic cell, which depend on several physical parameters such as lifetime of minority carriers, the intrinsic carrier density, coefficient of diffusion of electrons in the semiconductor, and others. This type information are not usually available in practical photovoltaic arrays. In this project the nominal saturation current $I_{0,n}$ is indirectly obtained from the experimental data through (5.5), which is obtained by evaluating (5.1) at the nominal open-circuit condition, with V = $V_{oc,n}$, I = 0, and I_{pv} H ≃ $I_{sc,n}$.

The value of the diode constant a may be randomly chosen. Usually 1 ≤ a ≤ 1.5 and the choice depends on other parameters of the I-V model its found by many other authors in their research. Some values are found based on empirical analysis. As [24] says, there are different opinions about the best way to choose a. Because an expresses the degree of ideality of the diode and it is totally empirical, any initial value of a can be chosen in order to adjust the model. In, order to improve the model fitting if necessary the value of a can be changed.

A. Improving The Model

The photovoltaic model described in the previous section can be improved if equation (5.10) is replaced by

$$I_o = \frac{I_{sc,n} + K_I\Delta T}{\exp\left(\frac{V_{OC,n} + K_V\Delta T}{aV_t}\right)-1} \quad ...(5.6)$$

This modification objective is to match the open-circuit voltages of the model with the experimental data for a very large range of temperatures. Eq. (5.6) is obtained from (5.2) by including in the equation the current and voltage coefficients K_V and K_I. The saturation current I_0 is strongly dependent on the temperature and (5.6) proposes a different approach to express the dependence of I_0 on the temperature so that the overall effect of the temperature is the linear variation of the open circuit voltage according the practical voltage/temperature coefficient. Simplifies the model and cancels the model error at the vicinities of the open-circuit voltages and consequently at other regions of the I-V curve by this equation.

The voltage/ temperature coefficient K_V brings important information necessary to achieve the best possible I-V curve fitting for temperatures different of the nominal value.

It is possible to obtain the best value of Eg for the model so that the open-circuit voltages of the model are matched with the open-circuit voltages of the real array in the range $T_n < T < T_{max}$. By equaling (5.4) and (5.6) and solving for Eg at T = T_{max} one gets

$$Eg = -\ln\left[\frac{\left(I_{sc,\,T\,\max}\right)\left(\frac{T_n}{T_{\max}}\right)^3}{\exp\left(\frac{qV_{oc,\,T\,\max}}{aN_s kT_{\max}}\right)-1}\right] * \frac{akT_n T_{\max}}{q(T_n - T_{\max})}$$

...(5.7)

where $I_{sc}, T_{max} = I_{sc,n} + K_I \Delta T$ and V_{oc}, $Tmax = V_{oc,n} + K_V \Delta T$, with $\Delta T = T_{max} - T_n$.

CONTROLLERS

There are three main aspects in the proposed converter's control: 1) During normal operation, a fixed duty cycle is used to control the TIBC MOSFETs, thus generating an unregulated high bus voltage for the inverter; 2) an MPP tracking (MPPT) algorithm is used along with a FUZZY controller to set the speed of the motor and achieve the energy balance of the system at the MPP of the PV module; and 3) a hysteresis controller is used during the no-load conditions and start-up of the system. Each of these aspects is described in the following sections.

Figure 6.1: Controller Block Diagram

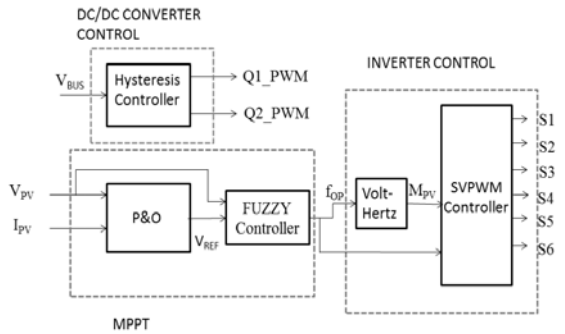

A. Fixed Duty Cycle

One of the most essential control aspects of this system is the fact that it is possible to use an unregulated dc output voltage and a fixed duty cycle for the first-stage dc/dc converter. As a resonant converter, there are definite time intervals in the switching period for the resonance process to occur. If altering the duty cycle or the switching period to control the output voltage, the converter may no longer operate at ZCS condition. Therefore these, design problem overcome the fixed duty cycle is used and ensure that the converter is going to operate in ZCS condition despite the input voltage or output load. The duty cycle was chosen to guarantee that the amount of transferred energy occurs during most part of the switching interval. Therefore, it is possible to transfer the same amount of energy with a smaller rms current. Therefore, the losses in the input inductors (*Li*1 and *Li*2), in the MOSFETs (*Q*1 and *Q*2), and in the transformer are lesser. As a result, the efficiency of the converter improves. Converter work with a constant voltage gain *Kv* due to operation with a fixed duty cycle makes the, almost independent of the input voltage. With the correct design of *Kv*, the system will always be capable to transfer energy from the PV module to the motor. Assuming that the converter is always operating at the MPP of the solar panel, the output dc/dc converter voltage (dc bus voltage) will be

$$V_{BUS} = V_{MPP*}K_v \qquad ...(6.1)$$

with, V_{MPP} being the MPP voltage of the solar panel.

On the other hand, it is necessary to analyze the minimum dc voltage on the inverter dc bus thus necessary to drive the motor at a specific power level. For this the volt/hertz controller was used to maintain approximately constant the pump's motor flux. The controller maintains the capability of the motor to generate nominal torque at any speed below its rated value by controlling

through volt/hertz. By neglecting the effect of rotor slip in induction machines and considering that the centrifugal water pump has its torque proportional to the square of the motor speed and that the frequency (f) in the volt/hertz control is proportional to the voltage (V), the motor output power (P) can be expressed as a cubic function of the motor voltage.

This minimum dc bus voltage was calculated by considering that the inverter is operating at the maximum voltage with a modulation index of 1 (no over modulation is allowed). The correct design of K_v assures that the output voltage of the first stage will always be greater than the minimum voltage necessary to drive the motor. The inverter provides a maximum line voltage equal to the bus voltage by using the SPWM strategy with third harmonic voltage injection. For a three-phase pump with V_{rms} as nominal line voltage, the gain K_v can be calculated by

$$K_v = \frac{V_{rms} * \sqrt{2}}{V_{MPP,\max}} \quad ...(6.2)$$

B. Hysteresis Controller

The main disadvantage of the classical TIBC is its inability to operate with no load or even in low-load conditions. The TIBC input inductors are charged even if there is no output current, and the energy of the inductor is lately transferred to the output capacitor raising its voltage indefinitely until its breakdown.

Normally, the input MOSFET cannot be turned off because there is no alternative path for the inductor current. With the addition of the proposed snubber, the TIBC switches can be turned off. Thus, a hysteresis controller can be set up based on the dc bus voltage level. Every time a maximum voltage limit is reached, indicating a low-load condition, this mode of operation begins. At this situation, the switches are turned off until the dc bus voltage returns to a normal predefined level.

Hysteresis controls also known as bang-bang control or ripple regulator control, maintains the converter output voltage within the hysteresis band centered about the reference voltage. The hysteretic-controlled regulator is popular because of its inexpensive, simple and easy-to-use architecture. The greatest benefits of hysteresis control are that it offers fast load transient response and eliminates the need for feedback-loop compensation. The other well-known characteristics are the varying operating frequency.

C. MPPT

The photovoltaic system has a non-linear current-voltage and power-voltage characteristics that continuously varies with irradiation and temperature. In order to track the continuously varying maximum power point of the solar array the MPPT (maximum power point tracking) control technique plays an important role in the PV systems. The task of a maximum power point tracking (MPPT) network in a photovoltaic (PV) system is to continuously tune the system so that it draws maximum power from the solar array regardless of weather or load conditions.

The MPPT is a strategy used to ensure that the operating point of the system is kept at the MPP of the PV panel. The Perturb and Observe was applied due to its simple implementation and fast dynamic response. This MPPT technique is based on the shape of the power curve of the PV panel. This curve can be divided into two sides, to the right and to the left of the MPP. By analyzing the voltage and power of the PV regularly it deduces the side of the PV panel

produces maximum power output point. The main idea of this method is to push the system to operate at the direction which the output power obtained from the PV system increases. If the change of power is positive, the system will keep the direction of the incremental current (increase or decrease the PV current) as the same direction, and if the change is negative, the system will change the direction of incremental current command to the opposite direction. This method works well in the steady state condition.

D. Fuzzy Controller

Fuzzy logic is one of the most powerful control methods and also known by multi-rules-based resolution and multivariable consideration. Fuzzy logic controllers (FLC) have the advantages of working with imprecise inputs, no need to have accurate mathematical model, and it can handle the nonlinearity [4]. The proposed FLC it consists of two inputs and one output. The two FLC input variables are the error (E) and change of error (CE) that expressed by equation as

$$E(j)=\frac{P_{PV}(j)-P_{PV}(j-1)}{V_{PV}(j)-V_{PV}(j-1)} \quad ...(6.3)$$

$$CE(j)=E(j)-E(j-1) \quad ...(6.4)$$

Table 6.1: Fuzzy Logic Table

E↓\CE→	NB	NS	ZE	PS	PB
NB	ZE	ZE	PB	PB	PB
NS	ZE	ZE	PS	PS	PS
ZE	PS	ZE	ZE	ZE	NS
PS	NS	NS	NS	ZE	ZE
PB	NB	NB	NB	ZE	ZE

where Ppv, Vpv are the PV power and voltage respectively at instant j. E (j) shows that load operating point at the instant j is located on the left or on the right of the maximum power point on the P-V characteristic. Where it is equals to zero at MPP while the change of error CE (j) expresses the moving direction of this point. Where the control action duty cycle D used for the tracking of the maximum power point by comparing with the saw tooth waveform to generate a PWM signal for the three phase voltage source inverter.

Based on the fuzzy logic table input 1, input 2 are set in fuzzy editor. Inputs are error and change in error and output is duty cycle for inverter.

Figure 6.1: Input 1

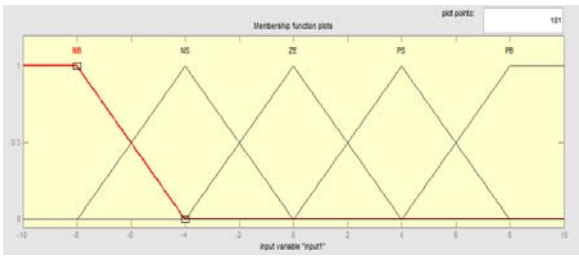

Figure 6.2: Input 2

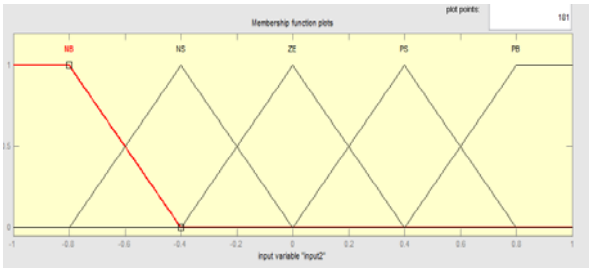

Figure 6.3: Input 3

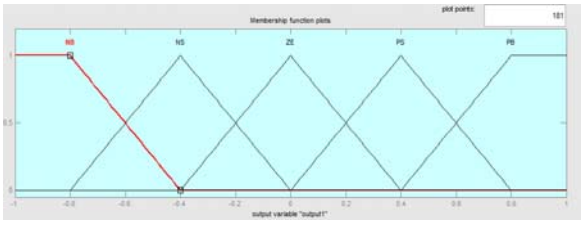

RESULTS AND DISCUSSION

Proposed system is verified with the MATLAB/ SIMULINK.

Photovoltaic cell PV curve and IV curve for irradiation of 700w/m^2.

This Figures 7.1 and 7.2 shows, voltage of PV panel is of 31 Volts, current is about 9.3 Amps and power achieved is 293 watts.

Figure 7.1: PV Curve

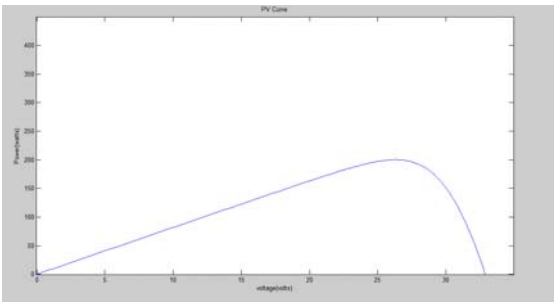

Figure 7.2: IV Curve

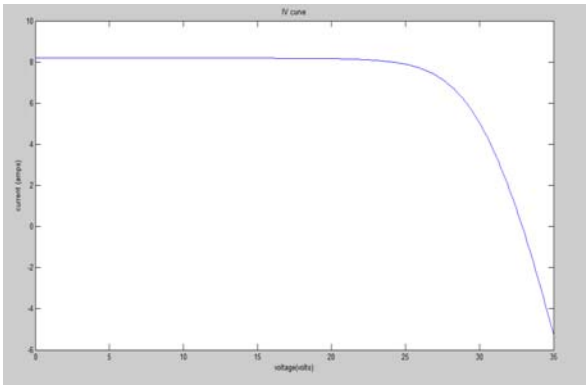

This Figure 7.3 provides the TIBC converter output voltage.

And Figure 7.4 shows that the output of three phase inverter voltage and current without respect to time.

This Figure 7.5 provides, speed of induction motor with respect to time.

Figure 7.3: Converter Output Voltage

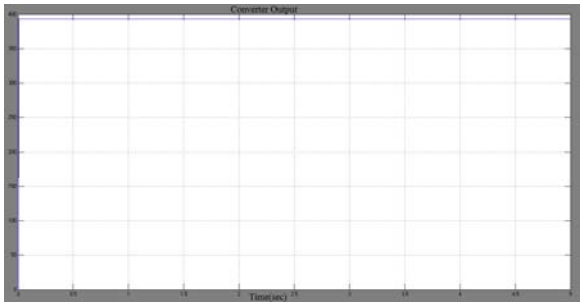

Figure 7.4: Voltage Source Inverter Voltage and Current

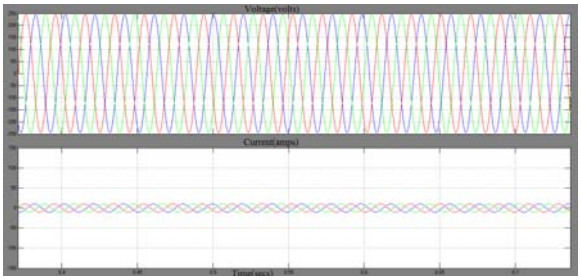

Figure 7.5: Induction Motor speed

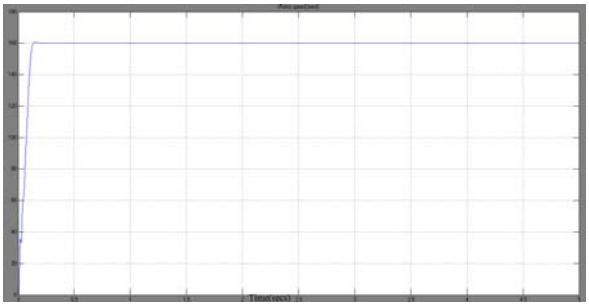

And this Table 7.1 provides, detail about the power factor, THD, and Settling time of motor speed for Fuzzy and MPPT P&O method and

Parameters	PI & Hill Climbing MPPT	Fuzzy & Perturb and Observe MPPT
Power Factor	0.95	0.97
Settling time of motor speed	0.24 sec	0.136 sec
THD	3.90 %	1.52 %

also shows the comparison result with PI and MPPT hill climbing algorithm.

CONCLUSION AND FUTURE WORK

The proposed converter provides the best solution for the application of water pumping from the solar PV without storage battery. Converter directly runs induction motor from solar energy. The proposed control enhanced the efficiency of the whole system. Comparison results showed that, the proposed method with Fuzzy achieved better performance than PI control method. Future scope work is to change the MPPT controller from P&O to incremental conductance method to overcome the disadvantage of P&O technique.

REFERENCES

1. João Victor Mapurunga Caracas (2014), Student Member, IEEE, Guilherme de Carvalho Farias, Student Member, IEEE, Luis Felipe Moreira Teixeira, Student Member, IEEE, and Luiz Antonio de Souza Ribeiro, Member, IEEE,"Implementation of a High-Efficiency, High-Lifetime, and Low-Cost Converter for an Autonomous Photovoltaic Water Pumping System" , IEEE Transactions On Industry Applications, Vol. 50, No. 1, pp. 631 – 641.
2. Villalva M G, Gazoli J R, Ruppert E F (2009), "Modeling And Circuit-Based Simulation Of Photovoltaic Arrays" , *Brazilian Journal of Power Electronics*, University of Campinas - UNICAMP, Vol. 14, No. 1, pp. 35-45, ISSN 1414-8862.
3. Ibrahim H E A (2012), "Comparison Between Fuzzy and P&O Control for MPPT for Photovoltaic System Using Boost Converter", *Journal of Energy Technologies and Policy* ISSN 2224-3232 (Paper) ISSN 2225-0573 (Online) Vol.2, No. 6, 2012, Dept. of Electrical and Computer Control Engineering Arab Academy for Science and Technology and marine transport, Cairo, Egypt.
4. Pongsakor Takun, Somyot Kaitwanidvilai and Chaiyan Jettanase (2011), "Maximum Power Point Tracking using Fuzzy Logic Control for Photovoltaic Systems" , Proceedings of the International Multi Conference of Engineers and Computer Scientists 2011 Vol II IMECS 2011, March 16-18, 2011, Hong Kong.
5. Chunting M, Correa M B R, and Pinto J O P (2010), "The IEEE 2011 international future energy challenge—Request for proposals," in *Proc. IFEC*, 2010, pp. 1–24.
6. Vitorino M A and Correa M B R (2009), "High performance photovoltaic pumping system using induction motor," in *Proc. Brazilian Power Electron. Conf.*, pp. 797–804.
7. Teröde G, Hameyer K, and Belmans R (1999), "Sensorless control of a permanent magnet synchronous motor for PV-powered water pump systems using the extended Kalman filter," in *Proc. 9th Int. Conf. Elect. Mach. Drives*, pp. 366–370.
8. Harsono H (2003), "Photovoltaic water pump system," Ph.D. dissertation, Dept. Intell. Mech. Syst. Eng., Faculty Kochi Univ. Technol., Kochi, Japan, Aug.
9. Tschanz D, Lovatt H, Vezzini A, and Perrenoud V (2010), "A multi-functional converter for a reduced cost, solar powered, water pump," in *Proc. IEEE ISIE*, pp. 568–572.
10. Vitorino M A, Correa M B R, Jacobina C B, and Lima A B N (2011), "An effective induction motor control for photovoltaic pumping," *IEEE Trans. Ind. Electron.*, Vol. 58, No. 4, pp. 1162–1170.

11. Cacciato M, Consoli A, and Crisafulli V (2010), "A high voltage gain dc/dc converter for energy harvesting in single module photovoltaic applications," in *Proc. IEEE ISIE*, pp. 550–555.
12. Wolfs P J (1993), "A current-sourced dc-dc converter derived via the duality principle from the half-bridge converter," *IEEE Trans. Ind. Electron.*, Vol. 40, No. 1, pp. 139–144, Feb.
13. Wolfs P and Li Q (2002), "An analysis of a resonant half bridge dual converter operating in continuous and discontinuous modes," in *Proc. IEEE Power Electron. Spec. Conf.*, 2002, pp. 1313–1318.
14. Liang T J, Chen R Y, Chen J F, and Tzeng W J (2007), "Buck-type current fed push-pull converter with ZCS for high voltage applications," in *Proc. IEEE Region 10 Conf.*, pp. 1–4.
15. Barbosa P M and Barbi I (1996), "A new current-fed, isolated PWM dc-dc converter," *IEEE Trans. Power Electron.*, Vol. 11, No. 3, pp. 431–438, May 1996.
16. Chen R Y, Liang T J, Chen J F, Lin R L, and Tseng K C (2008), "Study and implementation of a current-fed full-bridge boost dc-dc converter with zero-current switching for high-voltage applications," *IEEE Trans. Ind. Appl.*, Vol. 44, No. 4, pp. 1218–1226, Jul./Aug. 2008.
17. Kim J, Song H S, and Nam K (2011), "Asymmetric duty control of a dual half-bridge dc/dc converter for single-phase distributed generators," *IEEE Trans. Power Electron.*, Vol. 26, No. 3, pp. 973–982, Mar. 2011.
18. Yan L and Lehman B (2003), "Isolated two-inductor boost converter with one magnetic core," in *Proc. IEEE Appl. Power Electron. Conf. Expo.*, pp. 879–885.
19. Jang Y (2001), "Two-boost converter," U.S. Patent 6 239 584, May 29, 2001.
20. Li Q and Wolfs P (2006), "The power loss optimization of a current fed ZVS two-inductor boost converter with a resonant transition gate drive," *IEEE Trans. Power Electronics*, Vol. 21, pp. 1253–1263, Sep. 2006.
21. De Aragão Filho W C P and Barbi I (1996), "A comparison between two current-fed push-pull dc-dc converters—Analysis, design and experimentation," in *Proc. INTELEC*, 1996, pp. 313–320.
22. Yuan B, Yang X, Zeng X, Duan J, Zhai J, and Li D (2012), "Analysis and design of a high step-up current-fed multiresonant dc-dc converter with low circulating energy and zero-current switching for all active switches," *IEEE Trans. Ind. Electron.*, Vol. 59, No. 2, pp. 964–978, Feb. 2012.
23. Li D, Liu B, Yuan B, Yang X, Duan J, and Zhai J (2011), "A high step-up current fed multi-resonant converter with output voltage doubler," in *Proc. IEEE Appl. Power Electron. Conf. Expo.*, 2011, pp. 2020–2026.
24. Carrero C, Amador J, and Arnaltes S (2007), "A single procedure for helping PV designers to select silicon PV module and evaluate the loss resistances", *Renewable Energy.*
25. Glass M C (1996), "Improved solar array power point model with SPICE realization", In *Proc. 31st Intersociety Energy Conversion Engineering Conference, IECEC*, v. 1, p.286–291.
26. Yun Tiam Tan, Kirschen D S, and Jenkins N (2004), "A model of PV generation suitable for stability analysis", *IEEE Transactions on Energy Conversion*, Vol. 19, No. 4, pp. 748–755.

International Journal of Engineering Research and Science & Technology
Hyderabad, INDIA. Ph: +91-09441351700, 09059645577
E-mail: editorijlerst@gmail.com or editor@ijerst.com
Website: www.ijerst.com